

Influence of molecular symmetry on strong-field ionization: Studies on ethylene, benzene, fluorobenzene, and chlorofluorobenzene

Thomas K. Kjeldsen, Christer Z. Bisgaard, and Lars Bojer Madsen
Department of Physics and Astronomy, University of Aarhus, 8000 Århus C, Denmark

Henrik Stapelfeldt
Department of Chemistry, University of Aarhus, 8000 Århus C, Denmark

Using the molecular strong-field approximation we consider the effects of molecular symmetry on the ionization of molecules by a strong, linearly polarized laser pulse. Electron angular distributions and total ionization yields are calculated as a function of the relative orientation between the molecule and the laser polarization. Our studies focus on ethylene (C_2H_4), benzene (C_6H_6), fluorobenzene (C_6H_5F), and ortho chlorofluorobenzene (1,2 C_6H_4ClF), the molecules representing four different point groups. The results are compared with experiments, when available, and with the molecular tunneling theory appropriately extended to non-linear polyatomic molecules. Our investigations show that the orientational dependence of ionization yields is primarily determined by the nodal surface structure of the molecular orbitals.

PACS numbers: 33.80.Rv,33.80.Eh,82.50.Hp

I. INTRODUCTION

Ionization is an ubiquitous process in the interaction between atoms and molecules and intense laser fields. The ejected electron propagates in the combined laser and Coulomb field, and the laser field may steer back the electron and force it to recollide with the parent ion. In this way, the release of an electron into the laser-dressed continuum can initiate strong-field processes, such as above threshold ionization, multiple ionization, and high harmonic generation (see, e.g., Ref. [1] and references therein). Clearly, the laser field only drives the electron in the direction of the laser polarization vector and, consequently, rescattering dynamics is typically only present for linearly polarized laser fields. The possibility of rescattering depends not only on the parameters of the laser. Also the scattering angle with which the electron leaves the parent ion plays a role. For most atomic ground states, strong-field ionization leads to an outgoing electronic current in the direction of the linear polarization of the laser, and hence a recollision is possible after the field has changed its direction. For molecules, however, it happens, that the molecular symmetry imposes one or more nodal planes in the ground state wave function. In such planes the ejection of photoelectrons may be strongly suppressed [2], causing recollisionally induced double ionization not to peak for linearly but for elliptically polarized laser light [3]. It is therefore clear that a good understanding of the dependence of the initial ionization process upon laser parameters and upon parameters characteristic for the system, such as symmetry, is crucial for the further development and possible practical utilization of strong-field phenomena.

A large number of studies has established that the laser parameters determining strong-field ionization are the wavelength, the intensity, and the polarization [1, 4, 5, 6, 7]. We note in passing that in the case of few-

cycle laser pulses, the ionization rate and the photoelectron angular distribution also depends critically on the phase of the carrier frequency with respect to the envelope [8]. For atoms the most important system parameter is the binding energy of the initial state. In fact, the simple ADK tunneling model [9], employing only the laser intensity and the atomic binding energy as input parameters, provides for many atomic species a very good description of measured total ionization rates. Also, the theory referred to as the strong-field approximation (SFA) [10, 11, 12, 13, 14] has been successful in modeling atomic ionization including the angular distribution of the ejected photoelectrons. In this theory, the ionization takes place from a field-free ground state to a laser-dressed continuum final state via the interaction with the lowest-order laser-atom operator. In the final state, the Coulomb interaction between the electron and the parent ion is neglected and the electron is described by the state of a free electron in the laser field – the so-called Volkov state (see Ref. [15] for a very recent discussion).

For molecules a few recent studies have shown that there is an additional system parameter that also strongly influences strong-field ionization namely the symmetry of the initial electronic state [2, 16, 17, 18, 19, 20, 21, 22, 23]. Modifications of both the ADK tunneling theory [23] and the SFA [17] have been introduced to account for the molecular symmetry. Hereby the two models have provided results in reasonable agreement with measured ionization rates of molecules. In the molecular ADK (MO-ADK) theory [23] one expands the asymptotic molecular ground state wave function in a one-center basis and applies the atomic tunneling theory to each partial wave. The atomic SFA is straightforwardly generalized to the molecular SFA (MO-SFA) by using molecular wave functions. A very appealing feature of MO-SFA is that the expansion of the molecular wave function in linear combi-

nation of atomic orbitals (LCAO), allows an interpretation of the spectrum of photoelectrons in terms of interference from the multi-center molecule; an interpretation which in the context of single-photon ionization was offered almost 40 years ago [24].

In our previous work [2] we used the molecular strong-field approximation (MO-SFA) in the velocity gauge formulation to illustrate the strong dependence of the photoelectron angular distribution and the total ionization rates of ethylene and benzene on (i) the orientation between the molecule and the laser polarization and on (ii) the symmetry of the electronic wave function. The purpose of the present paper is to give a more thorough discussion of the influence of molecular symmetry on strong-field ionization. In particular, we study four different molecules representing four different classes of symmetry (point groups). We show how a reduction of the molecular symmetry lifts the degeneracy of molecular orbitals and leads to different ionization channels with distinct features.

More recently, we found that the MO-SFA in the velocity gauge formulation failed to explain orientational effects in ionization of N_2 . However, using the length-gauge to describe the molecule-field interaction, results in good agreement with experiments [16] were obtained [20]. Consequently, in the present work we found it necessary to employ both gauges and check if the results obtained are consistent. In addition, we calculate ionization rates by the MO-ADK tunneling model and compare with the results from the MO-SFA.

The paper is organized as follows. In Sec. II, we present a justification for using a Hartree-Fock calculation to represent the electronic ground states of the molecules under study. In Sec. III, we recall the theory of the MO-SFA and the MO-ADK tunneling models. In particular, we present the generalization of the MO-ADK theory [23] to the case of non-linear polyatomic molecules. In Sec. IV, we provide details of the calculations and discuss the choice of basis functions, the choice of nuclear coordinates, and the method for obtaining the ionization rates. In Sec. V, we present the numerical results comprising a comparison between the length and the velocity gauge. We argue that the length gauge gives the better results and use it together with the MO-ADK model to calculate ionization rates for each of the four molecules. In Sec. VI, we conclude and provide an outlook for the future.

II. ELECTRONIC STRUCTURE: HARTREE-FOCK OR BEYOND

In some molecules the inclusion of electron correlations is necessary in order to predict even qualitatively correct properties. For example, in N_2 the ordering of the orbitals obtained from a simple Hartree-Fock (HF) calculation is not consistent with the observed single-photon photoelectron spectrum: The calculated highest occupied molecular orbital (HOMO) of N_2 is a π_u orbital

while the HOMO inferred from experiments is a σ_g orbital [25]. When including electron correlations in the calculations, the correct ordering and ionization energies are obtained [26]. Another example where the effects of electron-electron correlation are important is F_2 which is not even bound in a HF treatment. It is therefore not surprising that one-electron models have failed in the attempt of explaining strong-field ionization of F_2 [17, 23, 27].

In this work, we consider ionization of ethylene and substituted benzenes. For these systems electron correlation may be safely neglected in the description of the initial state, since photoionization spectra in the valence region of these molecules consist of clearly separated bands which are unambiguously assigned and are in accordance with Hartree-Fock predictions [28, 29]. In these systems, each electron occupies an orbital obtained from a HF calculation and it is an accurate approximation to describe ionization by the removal of an electron from an occupied orbital while leaving the ion in an unrelaxed state. With these approximations, the many-electron problem translates into the much simpler single-electron problem. Only ionization from the highest or next highest occupied molecular orbital (referred to as HOMO-1) is considered. For ethylene and benzene the separations between the first and second ionization potential are 2.3 eV and 2.2 eV, respectively. In Ref. [30] it was shown that such large energy differences led to a much lower ionization probability from the HOMO-1 than from the HOMO. The separation between the first and second ionization potential is, however, much lower for the substituted benzenes, approximately 0.4 eV. Accordingly, we will consider ionization from the HOMO only for ethylene and the degenerate HOMO of benzene while for the substituted benzenes we will additionally include ionization from the HOMO-1. Ionization from all other orbitals is neglected.

III. THEORY

In this section, we describe the theories that we apply for the calculation of the molecular strong-field ionization. Throughout this work, we fix the nuclei at their equilibrium positions as determined with the HF theory.

A. Molecular strong-field approximation

The molecular strong-field approximation (MO-SFA) [2, 17, 20] is a generalization of the atomic strong-field approximation [10, 11, 12]. For a linearly polarized electric field $\mathbf{F}(t) = \mathbf{F}_0 \sin(\omega t)$ with associated vector potential $\mathbf{A}(t) = \mathbf{A}_0 \cos(\omega t)$, $A_0 = F_0/\omega$, the laser electron interaction is represented by [atomic units ($\hbar = m_e = e = a_0 = 1$) are used throughout]

$$V_F^{(LG)}(t) = \mathbf{r} \cdot \mathbf{F}(t), \quad (1)$$

in the length gauge (LG), and by

$$V_F^{(\text{VG})}(t) = \mathbf{A}(t) \cdot \mathbf{p} + \frac{\mathbf{A}^2(t)}{2}, \quad (2)$$

in the velocity gauge (VG).

In either gauge, we utilize the $2\pi/\omega = T$ periodicity of the field to express the angular differential, $dW/d\hat{\mathbf{q}}$, and total, W , ionization rates as sums of n -photon absorptions [20, 31]

$$\frac{dW}{d\hat{\mathbf{q}}} = 2\pi \sum_{n=n_0}^{\infty} |A_{qn}|^2 q_n, \quad (3)$$

$$W = 2\pi \sum_{n=n_0}^{\infty} \int |A_{qn}|^2 q_n d\hat{\mathbf{q}}, \quad (4)$$

where the transition amplitudes $A_{qn} =$

$1/T \int_0^T \langle \Psi_V(\mathbf{r}, t) | V_F^{(c)}(t) | \Psi(\mathbf{r}, t) \rangle dt$ ($c = \{\text{LG}, \text{VG}\}$) are evaluated at the momentum $q_n = \sqrt{2(n\omega - E_b - U_p)}$, with E_b the binding energy of the initially bound electron and U_p the ponderomotive potential. Energy conservation also determines the minimum number of photons needed to reach the continuum, i.e., the lower limit n_0 of the sum. In the expression for A_{qn} , Ψ_V is a $(2\pi)^{-3/2}$ normalized Volkov wave function and $\Psi(\mathbf{r}, t)$ the wave function for the electron in the combined field of the molecule and the laser. Introducing the strong-field approximation, i.e., $\Psi(\mathbf{r}, t) \simeq \Psi_0(\mathbf{r}, t) = e^{iE_b t} \Phi_0(\mathbf{r})$, with Φ_0 the solution of the time-independent field-free HF equation, we find the length and velocity gauge amplitudes [20, 31]

$$A_{qn}^{(\text{LG})} = \frac{1}{T} \int_0^T dt \left(-E_b - \frac{Q_n^2(t)}{2} \right) \tilde{\Phi}_0(\mathbf{Q}_n(t)) \exp i \left(n\omega t + \mathbf{q}_n \cdot \boldsymbol{\alpha}_0 \sin(\omega t) + \frac{U_p}{2\omega} \sin(2\omega t) \right), \quad (5)$$

$$A_{qn}^{(\text{VG})} = \left(-E_b - \frac{q_n^2}{2} \right) \tilde{\Phi}_0(\mathbf{q}_n) \frac{1}{T} \int_0^T dt \exp i \left(n\omega t + \mathbf{q}_n \cdot \boldsymbol{\alpha}_0 \sin(\omega t) + \frac{U_p}{2\omega} \sin(2\omega t) \right). \quad (6)$$

Here $\mathbf{Q}_n(t) = \mathbf{q}_n + \mathbf{A}(t)$ denotes the time-dependent momentum, $\boldsymbol{\alpha}_0 = \mathbf{A}_0/\omega$ denotes the quiver radius, and $\tilde{\Phi}_0(\mathbf{q}) = (2\pi)^{-3/2} \int d\mathbf{r} e^{-i\mathbf{q}\cdot\mathbf{r}} \Phi_0(\mathbf{r})$ the momentum wave function of the initially bound electron. The velocity gauge transition amplitude of Eq. (6) may be simplified by replacing the time integral with a generalized Bessel function $J_n(u, v)$ [12] and using energy conservation

$$A_{qn}^{(\text{VG})} = (U_p - n\omega) \tilde{\Phi}_0(\mathbf{q}_n) J_{-n} \left(\mathbf{q}_n \cdot \boldsymbol{\alpha}_0, \frac{U_p}{2\omega} \right). \quad (7)$$

Applying Eq. (7) to the differential rate of Eq. (3) is equivalent to the expression used in Ref. [17]. We note that Eq. (5) simplifies to Eq. (6) when neglecting $\mathbf{A}(t)$ compared to \mathbf{q}_n , i.e., when $\mathbf{Q}_n(t) \approx \mathbf{q}_n$.

We construct the molecular one-electron wave functions as linear combinations of basis functions ϕ_{ij} based on each atom (LCAO-MO), located at the positions \mathbf{R}_i . The wave function can now be written as

$$\Phi_0(\mathbf{r}, \{\mathbf{R}_i\}) = \sum_{i=1}^N \sum_{j=1}^{j_{max}^{(i)}} a_{ij} \phi_{ij}(\mathbf{r} - \mathbf{R}_i), \quad (8)$$

where i runs over the N atoms in the molecule and j runs over the basis functions on each atom ϕ_{ij} . The Fourier

transform of the wave function is then

$$\tilde{\Phi}_0(\mathbf{q}_n) = \sum_{i=1}^N \sum_{j=1}^{j_{max}^{(i)}} a_{ij} \tilde{\phi}_{ij}(\mathbf{q}_n) e^{-i\mathbf{q}_n \cdot \mathbf{R}_i}, \quad (9)$$

with $\tilde{\phi}_{ij}$ representing ϕ_{ij} in momentum space.

B. Molecular tunneling theory

The molecular ADK (MO-ADK) tunneling theory [19, 23] is a generalization of the atomic ADK theory [9]. In previous works [19, 20, 23] the MO-ADK theory was applied to diatomic molecules. Here the theory is generalized to cover also nonlinear polyatomic molecules.

The tunneling theory relies on the assumption that at any given instants of time the molecule will respond to the external laser field as if it were a static electric field. The rate of ionization in the oscillating field may thus be determined by the time-averaged static rates. Whether this approach is reasonable or not depends on the value of the Keldysh parameter $\gamma = \sqrt{2E_b} \frac{\omega}{F_0}$ [10] with $\gamma \ll 1$ in the tunneling regime.

The formulation of a tunneling theory in the case of molecules is complicated compared to the atomic case by two related features. Firstly, the presence of multiple nuclei within the molecule breaks the spherical symmetry

of the field-free system and necessitates a description of the molecular wave function in terms of a superposition of partial waves. Secondly, the Euler angles describing the orientation between the laboratory fixed frame (with a Z -axis determined by the linear polarization vector of the external field) and the molecular body fixed frame have to be specified. Note that we use (X, Y, Z) to label the laboratory fixed frame of reference and (x, y, z) to label the body-fixed frame of reference. The tunneling rate of molecules can be determined once the field-free asymptotic wave function is known. In a body-fixed frame, labeled by superscript B , this function must follow the asymptotic Coulomb form

$$\Phi_0^B(\mathbf{r}) \sim r^{Z_{\text{ion}}/\kappa-1} e^{-\kappa r} \sum_{l,m} C_{lm} Y_{lm}(\hat{\mathbf{r}}), \quad (10)$$

where Z_{ion} is the charge of the residual ion and κ is related to the binding energy, $\kappa = \sqrt{2E_b}$. For the tunneling process in the DC case, we assume the electric field to point in the positive Z -direction, corresponding to a situation where tunneling would occur in the negative Z -direction. Consequently, we need to express the asymptotic form of the molecular wave function in that direction. If the body-fixed frame is rotated by the Euler angles (ϕ, θ, χ) with respect to the laboratory fixed system, the asymptotic form in the laboratory fixed system of the field-free molecular ground state wave function is expressed through the rotation operator $\hat{D}(\phi, \theta, \chi)$ as $\Phi_0^L(\mathbf{r}) = \hat{D}(\phi, \theta, \chi) \Phi_0^B(\mathbf{r})$, where we have used the superscript L to denote the laboratory fixed system. Equation (10) then leads to the expression

$$\Phi_0^L(\mathbf{r}) \sim r^{Z_{\text{ion}}/\kappa-1} e^{-\kappa r} \sum_{l,m} C_{lm} \sum_{m'} \mathcal{D}_{m'm}^{(l)}(\phi, \theta, \chi) Y_{lm'}(\hat{\mathbf{r}}), \quad (11)$$

where $\mathcal{D}_{m'm}^{(l)}(\phi, \theta, \chi)$ is a Wigner rotation function [32, 33]. In Eq. (11) the sum over m' and the corresponding Wigner functions describes the rotation between the coordinate systems and the sum over l, m is a signature of the breaking of the spherical symmetry by the molecular system. For linear molecules the projection m of the electronic angular momentum onto the body-fixed axis is a good quantum number and, hence, for such systems there would be no summation over m in Eqs. (10) and (11) [23]. For later convenience, we note that ϕ and χ represent rotations around the space-fixed Z -axis and the body fixed z -axis, respectively, while θ represents the angle between the Z and z axes.

From the asymptotic form of Eq. (11), the total ionization rate in a static (DC) field in the positive Z direction is calculated as in the atomic case [34, 35, 36], and the result is

$$W_{\text{stat}}(F_0) = \sum_{m'} \frac{|B(m')|^2}{2^{|m'|} |m'|! \kappa^{2z/\kappa-1}} \times \left(\frac{2\kappa^3}{F_0} \right)^{2Z/\kappa-|m'|-1} \exp\left(-\frac{2}{3} \frac{\kappa^3}{F_0}\right), \quad (12)$$

where

$$B(m') = \sum_{l,m} (-1)^{(|m'|+m')/2} \sqrt{\frac{(2l+1)(l+|m'|)!}{2(l-|m'|)!}} \times C_{lm} \mathcal{D}_{m'm}^{(l)}(\phi, \theta, \chi). \quad (13)$$

In a slowly varying field, the ionization rate is found by averaging the DC rate over an optical cycle

$$W = \frac{1}{2\pi} \int_0^{2\pi} W_{\text{stat}}(F_0 \cos(\omega t)) d(\omega t). \quad (14)$$

The DC rate is given by Eq. (12) when the field is oriented in the positive Z direction, $|\pi - \omega t| \geq \pi/2$, corresponding to tunneling in the negative Z -direction. When the field points in the negative Z direction, $\pi/2 \leq \omega t \leq 3\pi/2$, corresponding to the possibility for tunneling in the positive Z -direction, the geometry is equivalent to a field pointing in the positive Z direction but with an inverted molecule. We account for this by applying the parity operator \mathcal{P} on the wave function Φ_0^B

$$\mathcal{P} \Phi_0^B(\mathbf{r}) \sim r^{Z_{\text{ion}}/\kappa-1} e^{-\kappa r} \sum_{l,m} C_{lm} (-1)^l Y_{lm}(\hat{\mathbf{r}}), \quad (15)$$

and we see by comparing with Eq. (10) that this simply corresponds to the substitution $C_{lm} \rightarrow (-1)^l C_{lm}$ in Eq. (13). Note that parity eigenstates, corresponding to inversion symmetric molecules, contain only even or odd l states. When the field direction is changed Eq. (13) will either remain invariant or change sign and the DC rate is thereby left invariant. Contrary, the DC rate will not be invariant to field inversion for states which are not parity eigenstates. This is also to be expected since the wave functions in the tunneling regions in the positive and negative Z direction will be different. Under the assumption $\kappa^3/F_0 \ll 1$ the integral in Eq. (14) may be approximated by

$$W = \sqrt{\frac{3F_0}{\pi\kappa^3}} \frac{W_{\text{stat}}^+(F_0) + W_{\text{stat}}^-(F_0)}{2}, \quad (16)$$

where $W_{\text{stat}}^\pm(F_0)$ are the DC rates for the positive and negative field directions with respect to the Z direction.

IV. CALCULATIONS

A. Basis set

The Hartree-Fock wave functions for ethylene, benzene, fluorobenzene and *o*-chlorofluorobenzene are calculated using GAMESS [37] with a standard valence triple zeta basis set [38]. This basis set contains *s* and *p* orbitals for carbon, fluorine and chlorine while the hydrogen basis consists only of *s* orbitals. Since the tunneling rates and the length gauge MO-SFA rates both rely on the

asymptotic form of the wave function a precise description is needed in this region. This is obtained by adding an extra diffuse s and p basis function. The orbitals of the molecules considered are odd under reflection in their molecular planes. Thus the LCAO expansion, Eq. (8), can only include p orbitals orthogonal to the plane. For example, if we define the yz plane to coincide with the molecular plane, the relevant p orbitals are the p_x orbitals.

B. Expansion and asymptotic coefficients

The calculation of the initial molecular ground state wave function is performed at the equilibrium geometry predicted by Hartree–Fock theory. Bond lengths obtained in this way are typically within few pm from experimental data [39]. The nuclear geometries are shown in Fig. 1.

Note that we define the body-fixed z axis to be perpendicular to the molecular plane for benzene while it lies in the molecular plane for the remaining molecules. Since we want to investigate the influence of molecular alignment on the ionization rates, we have chosen our axes to coincide with the principal axes for each molecule. Aligned molecules are generated as superpositions of rotational eigenstates which are most conveniently described in this coordinate system [40]. Our definitions of coordinates are in accordance with the usual conventions except for chlorofluorobenzene.

The asymptotic form of the orbitals, Eq. (10), is found by expanding in spherical harmonics

$$\Phi_0(\mathbf{r}) = \sum_{l,m} F_{lm}(r) Y_{lm}(\hat{\mathbf{r}}), \quad (17)$$

leading to

$$F_{lm}(r) = \int d\Omega Y_{lm}^*(\hat{\mathbf{r}}) \Phi_0(\mathbf{r}). \quad (18)$$

These functions are then matched to the form $F_{lm}(r) \sim C_{lm} r^{Z_{\text{ion}}/\kappa-1} e^{-\kappa r}$ in the asymptotic region whereby the coefficients C_{lm} are determined. The values of C_{lm} for the molecules investigated in this work are given in Table I. All the orbitals are odd eigenstates of the σ_{yz} reflection operation and they are additionally chosen purely real. The projection on the spherical harmonics, Eq. (18), will then be either purely real (m odd) or purely imaginary (m even). Another consequence of the yz reflection antisymmetry is $F_{l,-m}(r) = -F_{l,m}(r)$. In ethylene, benzene and fluorobenzene our orbitals are additionally be eigenstates of the σ_{xz} reflection operation. If the wave function is an even (odd) eigenstate of the σ_{xz} reflection operation then only the real, m odd, (imaginary, m even) radial functions will occur.

Since the basis functions we use are Gaussian and the correct asymptotic form to which we fit, is exponential, we cannot expect a precise fit all the way to infinity.

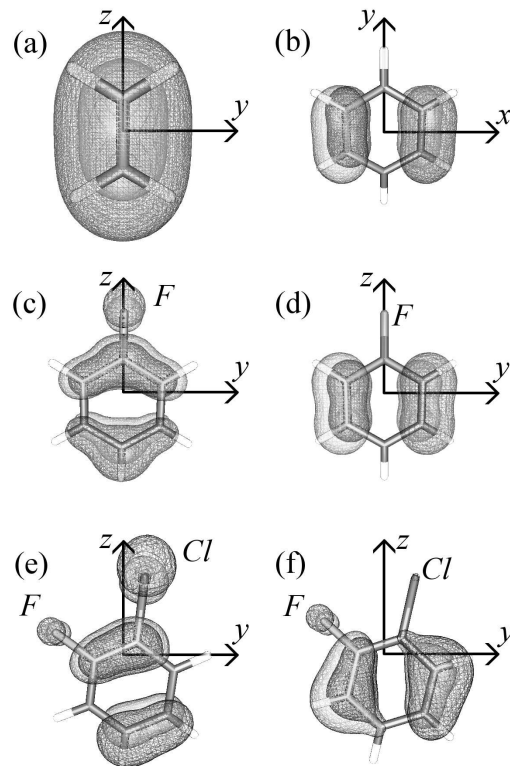


Figure 1: Nuclear geometries and isocontours for the active orbitals of (a) ethylene, (b) benzene, (c) and (d) HOMO and HOMO-1 for fluorobenzene respectively and (e) and (f) HOMO and HOMO-1 for 1,2-chlorofluorobenzene respectively. The origins of the coordinate systems are in the center-of-mass. For later convenience we see that all the orbitals contain nodal planes in the molecular plane. The HOMOs of fluorobenzene and 1,2-chlorofluorobenzene, (d) and (f), contain nodal surfaces which are approximately parallel to the xy plane. The HOMO-1 of fluorobenzene contains a nodal plane in the xz plane while the HOMO-1 of 1,2-chlorofluorobenzene contains a nodal surface which is almost in the xz plane. The relation between the body-fixed axes shown in the figures and the laboratory-fixed axes is discussed in Sec. III B.

Accordingly, we have adjusted the range of asymptotic fitting to start well outside the nuclear positions and is limited such that the radial functions $F_{lm}(r)$ of Eq. (18) still follow the exponential behavior. In Ref. [20], we obtained accurate results by this procedure.

C. Simplifications in the length gauge

In the length gauge MO-SFA the transition amplitude, will only depend on the asymptotic behavior of the coordinate space wave function [20, 31].

When we have determined the angular coefficients C_{lm} we may simply use the Fourier transform of Eq. (11) in the length gauge transition amplitude of Eq. (5). The

Table I: Asymptotic coefficients C_{lm} .

l	m	C_2H_4	C_6H_6	C_6H_5F		$1,2 C_6H_4ClF$	
				HOMO	HOMO-1	HOMO	HOMO-1
1	± 1	± 1.10		± 0.49		± 1.27	± 0.08
2	± 2				$\mp 1.70i$	$\mp 0.39i$	$\mp 1.39i$
	± 1		± 1.36	∓ 1.70		∓ 0.95	± 0.19
3	± 3			± 0.13		∓ 0.28	∓ 0.54
	± 2				$\pm 1.22i$	$\pm 0.39i$	$\pm 1.51i$
	± 1	± 0.22		± 0.89		± 1.83	∓ 0.71
4	± 4				$\pm 0.35i$	$\pm 0.10i$	$\pm 0.41i$
	± 3			± 0.24		± 0.13	± 0.16
	± 2				$\mp 0.68i$	$\mp 0.63i$	$\mp 0.75i$
	± 1		∓ 0.32	± 0.31		∓ 0.53	± 0.26
5	± 5					± 0.03	± 0.11
	± 4				$\mp 0.25i$	$\mp 0.10i$	$\mp 0.30i$
	± 3			∓ 0.11		∓ 0.21	∓ 0.01
	± 2				$\pm 0.33i$	$\pm 0.06i$	$\pm 0.30i$
	± 1			± 0.23		± 0.82	∓ 0.25
6	± 4				$\pm 0.16i$	$\pm 0.10i$	$\pm 0.18i$
	± 2				$\mp 0.12i$	$\mp 0.22i$	$\mp 0.10i$
	± 1					∓ 0.17	± 0.07

Fourier transform of Eq. (11) is

$$\tilde{\Phi}_0(\mathbf{q}) = \sum_l \tilde{f}_l(q) \sum_{m,m'} C_{lm} \mathcal{D}_{m'm}^{(l)}(\phi, \theta, \chi) Y_{lm'}(\hat{\mathbf{q}}), \quad (19)$$

where the radial momentum-space functions $\tilde{f}_l(q)$ are

$$\begin{aligned} \tilde{f}_l(q) &= 2\pi^{3/2} \left(-\frac{iq}{2}\right)^l \frac{\Gamma(l + \frac{Z}{\kappa} + 2)}{\kappa^{l+Z/\kappa+2} \Gamma(l + \frac{3}{2})} \\ &\times {}_2F_1\left(\frac{l + \frac{Z}{\kappa} + 2}{2}, \frac{l + \frac{Z}{\kappa} + 3}{2}; l + \frac{3}{2}; -\frac{q^2}{\kappa^2}\right), \end{aligned} \quad (20)$$

with ${}_2F_1(a, b; c; z)$ Gauss' hypergeometric function [41]. Equation (5) can now be rewritten as

$$\begin{aligned} A_{\mathbf{q}_n}^{(LG)} &= \sum_{l,m,m'} \mathcal{D}_{m'm}^{(l)}(\phi, \theta, \chi) C_{lm} \\ &\times \frac{1}{T} \int_0^T dt \left(-E_b - \frac{Q_n^2(t)}{2}\right) \tilde{f}_l(Q_n(t)) Y_{lm'}(\hat{\mathbf{Q}}_n(t)) \\ &\times \exp i \left(n\omega t + \mathbf{q}_n \cdot \boldsymbol{\alpha}_0 \sin(\omega t) + \frac{U_p}{2\omega} \sin(2\omega t) \right), \end{aligned} \quad (21)$$

with $\mathbf{Q}_n(t) = \mathbf{q}_n + \mathbf{A}(t)$. This formula is particularly useful when we want to consider many different molecular orientations, since the integrals in Eq. (21) are independent of molecular orientation. Firstly, we need to calculate all the integrals once for each l and m' at some lab fixed momentum \mathbf{q}_n . Then we can easily get the transition amplitude at the same lab fixed momentum for all

orientations (ϕ, θ, χ) by multiplication with the appropriate Wigner functions. We have checked this method against calculations with the fully numeric Fourier transforms applied in Eq. (5) and we find agreement within $\lesssim 20\%$ in the final rates.

In closing this section, we note that with the above simplifications of the length gauge MO-SFA, the only non-trivial dependency on electronic structure of the MO-SFA LG and the MO-ADK theory is through the C_{lm} expansion coefficients.

D. Ion signal

The ionization rates in Eqs. (4) and (14) depend on the instantaneous amplitude of the field and the molecular orientation described by the Euler angles (ϕ, θ, χ) . We only consider linearly polarized light and hence the results are independent of ϕ , the angle of rotation around the polarization vector. For a Gaussian laser beam with a Gaussian temporal profile with FWHM τ , the amplitude of the vector potential is

$$A(\mathcal{R}, \mathcal{Z}, t) = \frac{\sqrt{I_0}}{\omega} \frac{w_0}{w(\mathcal{Z})} e^{-\mathcal{R}^2/w(\mathcal{Z})^2} \exp\left(-\frac{2 \ln 2 t^2}{\tau^2}\right), \quad (22)$$

where $(\mathcal{R}, \mathcal{Z})$ are the cylindrical coordinates, I_0 the peak intensity, w_0 is the spot size and $w(\mathcal{Z}) = w_0 \sqrt{1 + \mathcal{Z}^2/\mathcal{Z}_R^2}$ where $\mathcal{Z}_R = \pi w_0^2/\lambda$ is the Rayleigh length and λ the wavelength.

The rate equations for the ionization probability of a molecule oriented according to the Euler angles (θ, χ) and located at $(\mathcal{R}, \mathcal{Z})$ in the laser focus are

$$\frac{dp_0}{dt} = -W(\mathbf{A}(\mathcal{R}, \mathcal{Z}, t), \theta, \chi) p_0 \quad (23)$$

$$\frac{dp_1}{dt} = W(\mathbf{A}(\mathcal{R}, \mathcal{Z}, t), \theta, \chi) p_0, \quad (24)$$

where p_0 and p_1 denote the probabilities of having a neutral or an ion, and ionization to higher charge states is neglected. By the end of the pulse, the solution to Eq. (23) is given by

$$p_1(\mathcal{R}, \mathcal{Z}, \theta, \chi) = 1 - \exp\left(-\int_{-\infty}^{\infty} W(\mathbf{A}(\mathcal{R}, \mathcal{Z}, t'), \theta, \chi) dt'\right). \quad (25)$$

The orientational dependent number of ionized molecules N_1 is found by integrating Eq. (25) over the beam profile

$$N_1(\theta, \chi) = 2\pi\rho \int \mathcal{R} d\mathcal{R} \int d\mathcal{Z} p_1(\mathcal{R}, \mathcal{Z}, \theta, \chi), \quad (26)$$

where ρ is the constant density of the target gas. In experiments it is difficult to measure the absolute yield due to unknown detection efficiency. The measured ion signal is, however, proportional to the number of ionized molecules. Measured ratios of yields for different molecular orientations are thus independent of detection efficiency. We note that the actual evaluation of the integral

Eq. (25) can be simplified by integrating over iso-intensity shells [42]. This method describes experiments in which all ionized molecules are measured.

V. RESULTS AND DISCUSSION

To justify the use of the approximate theories discussed in Sec. III, we first calculate the intensity dependent ion signal for ethylene and benzene and compare with experimental data. Previous studies using the velocity gauge MO-SFA have shown that the absence of the final state Coulomb interaction in this model will underestimate the ionization rates. To take this interaction into account a correction factor $C_{\text{Coul}}^{(v)} = (\kappa^3/F_0)^{2Z_{\text{ion}}/\kappa}$ was proposed [17]. In our velocity gauge calculations, we adopt this correction factor. A recent study on N_2 [20] revealed that the effect of the Coulomb interaction is much smaller with the length gauge MO-SFA. The explanation is that the combined laser-ion interaction with the electron is already present through the factor $\hat{\Phi}_0(\mathbf{q}_n + \mathbf{A}(t))$ in Eq. (5) and also in the length gauge, the ionization occurs at large distances from the core. In this spatial region, the Coulomb interaction is already suppressed compared to the electron-laser interaction. Below we demonstrate that the length gauge MO-SFA without any extra Coulomb correction factor reproduces experimental ion signals of C_2H_4 and C_6H_6 .

For direct comparison of results obtained by MO-SFA and MO-ADK theories with the experimental data it is necessary to express the total rate of ionization as the sum of rates leading to unresolved final states. This means that the rates in Eqs. (3) and (4) must be multiplied by the number of electrons which occupy the active orbital, i.e., 4 for the degenerate HOMO of benzene and 2 for the non-degenerate closed shell orbitals.

Figures 2 and 3 show theoretical results and experimental data of the ion signal versus peak intensity for experiments on ethylene and benzene, respectively. The calculations are the MO-ADK, the length gauge MO-SFA (MO-SFA LG) and the velocity gauge MO-SFA (MO-SFA VG). Following the discussion in Sec. IV D, we normalize the results of each calculation to match the experimental data at high intensities. The figures show that the MO-SFA LG predicts results in excellent agreement with both the ethylene and the benzene experimental data. The Coulomb corrected MO-SFA VG results fit the data reasonably well, while we find a poor agreement between the MO-ADK model and experiments. We explain this latter discrepancy by the fact that the intensities considered here do not strictly correspond to the tunneling regime. Typical values of the Keldysh parameter are 3.0 (2.8) for ethylene (benzene) at $I_0 = 10^{13} \text{ Wcm}^{-2}$ and 0.94 (0.88) at $I_0 = 10^{14} \text{ Wcm}^{-2}$. We note that despite both MO-SFA models are in agreement with these total ion-yield experiments, a recent study on orientational-dependent ionization from N_2 showed that the length gauge formulation is the better choice [20].

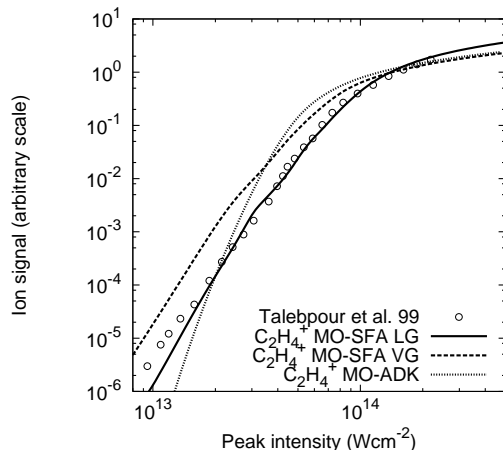


Figure 2: Ion signal for ethylene at 800 nm versus the peak intensity of the laser. The laser wavelength is 800 nm, the beam waist is $49 \mu\text{m}$ and the pulse duration (FWHM) is 200 fs. Experimental data are from Ref. [43]. The solid line indicates the length gauge MO-SFA (MO-SFA LG) predictions, the long-dashed line shows the velocity gauge MO-SFA (MO-SFA VG) predictions and the short-dashed line shows predictions of MO-ADK theory.

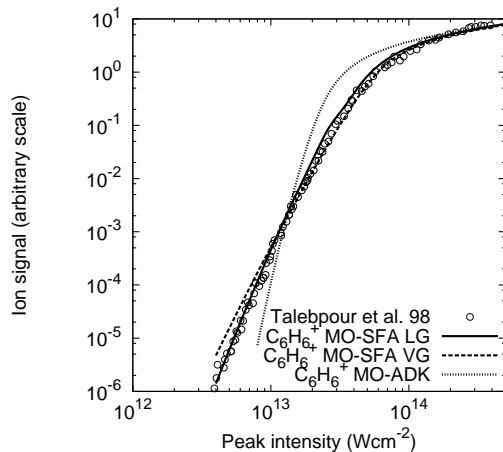


Figure 3: Similar to Fig. 2 but for benzene. Experimental data are from Ref. [44].

A. Ethylene

The main conclusion from our earlier velocity gauge work on ethylene [2] was that the angular distributions of photoelectrons are very sensitive to the relative orientation between the laser polarization and the molecule. This could be interpreted as an effect of the nodal plane structure of the HOMO. Electron emission was found to

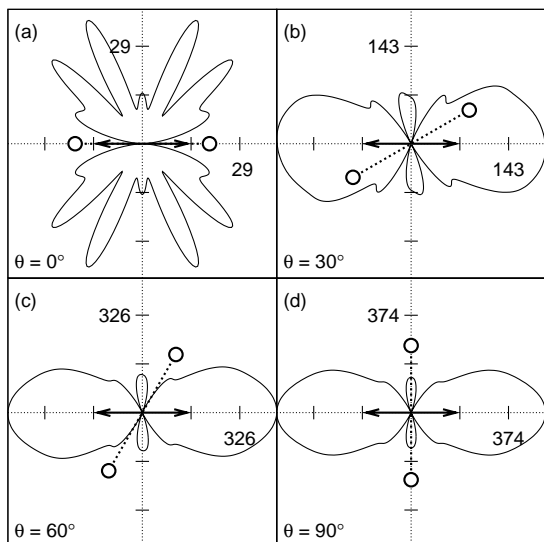


Figure 4: (a)–(d) Polar plots of the angular differential ionization rate of ethylene by an 800 nm, $5 \times 10^{13} \text{ Wcm}^{-2}$ field using the length gauge MO-SFA. Rates are in units of 10^{10} s^{-1} . The polarization (double headed arrow) is horizontal and the molecular plane is perpendicular to the paper with the C–C axis (dotted line) in the plane of the paper ($\chi = 0^\circ$) and (a) $\theta = 0^\circ$, (b) 30° , (c) 60° , (d) 90° .

be impossible in the directions of the molecular plane which led to a suppression of the total ionization rate when the molecular plane coincided with the polarization vector.

We first present polar plots of angular differential ionization rates using the length gauge MO-SFA (Fig. 4) and the Coulomb corrected velocity gauge MO-SFA (Fig. 5) for different molecular orientations, specified by the angle θ between the polarization and the body-fixed z axis defined in Fig. 1 (a). Our primary purpose of these calculations is to check if the results in the two gauges are compatible. From Figs. 4 and 5 we see that both models predict an increase in the ionization rate as the polar angle θ increases. When the molecular plane coincides with the polarization, the rates are strongly suppressed and in both models no electron emission is observed along the polarization direction. In the velocity gauge this phenomenon was explained by the presence of a nodal plane in the molecular plane [2]. There is a one-to-one correspondence between nodal planes in coordinate space and momentum space. Thus, the velocity gauge transition amplitude, Eq. (6), vanishes at momenta which lie in the nodal plane. This is indeed what we observe in Fig. 5. In the length gauge transition amplitude, Eq. (5), the momentum wave function is not evaluated at the actual outgoing momentum but at a time-dependent displaced momentum $\mathbf{q}_n + \mathbf{A}(t)$. This has the consequence that even though \mathbf{q}_n lies in the nodal plane the transition amplitude can be nonzero. Only when \mathbf{q}_n and $\mathbf{A}(t)$ both lie in the nodal plane ($\theta = 0^\circ$) the transition amplitude is

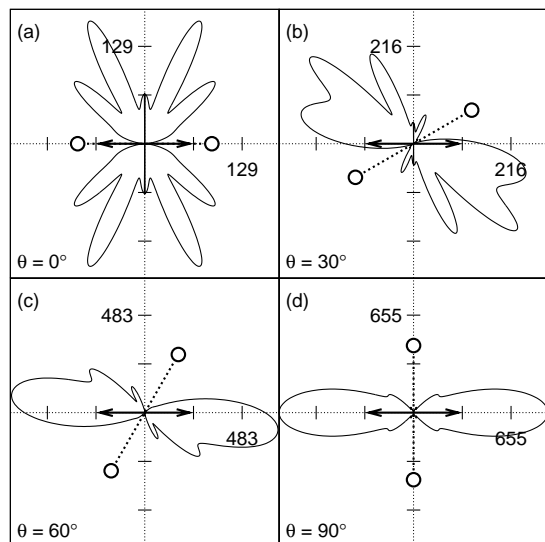


Figure 5: Similar to Fig. 4 but calculated in velocity gauge.

zero. This argument is general for molecules which ionize from orbitals containing nodal planes. In both gauges the ionization rate is thus expected to be suppressed for molecular orientations with the polarization coinciding with a nodal plane. This leads to the qualitative agreement in the two gauges. For molecules without planar nodal surfaces no such suppressions can *a priori* be expected for any geometry. Based on previous work on strong-field ionization of N_2 [20] and detachment of negative ions [31, 45] we judge that the length gauge is the proper choice of gauge to use in the strong-field approximation. Accordingly, in the calculations below we will only use the length gauge MO-SFA.

Currently, angle resolved photoelectron measurements on aligned molecules have not been performed. However, the first measurements of total ion yields on aligned molecules have been reported [16]. In order to make prediction on these types of experiments we show in Fig. 6 the total ion yield as a function of molecular orientation using (a) the MO-SFA LG model and (b) the MO-ADK model. The figure shows the yields which would be measured if all molecules were oriented according to the Euler angles specified. Explicitly, we show the signals as a function of the polar angle θ for two specific χ angles with all signals being normalized to the $\theta = 0^\circ$ geometry. We recall that $\theta = 0^\circ$ for the molecular plane parallel with the linear polarization, and $\theta = 90^\circ$ for the perpendicular geometry. In experiments, utilizing linearly polarized light pulses for the alignment, the molecular axis with largest polarizability is aligned along the polarization direction [46] (the C–C axis for ethylene). In this case the molecule is free to rotate around its body-fixed z axis and measured signals are thus a result of an average over the χ angle. Correspondingly, we have calculated the χ averaged signal too.

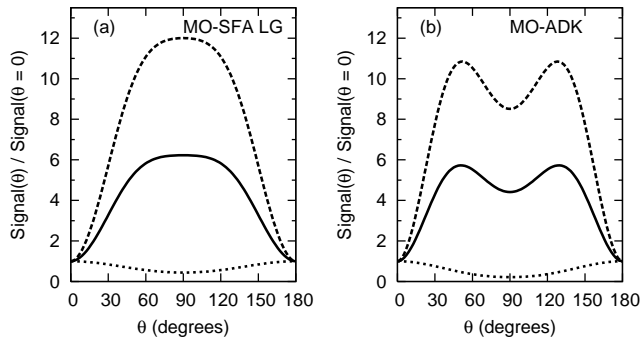


Figure 6: The orientational dependent ion signal for ionization from ethylene using (a) the molecular strong-field approximation in the length gauge formulation and (b) the molecular tunneling theory. The signal is given as a function of the polar angle θ with $\chi = 0^\circ$ (long dashed), $\chi = 90^\circ$ (short dashed) and χ averaged (solid). The parameters of the laser are: $\lambda = 800$ nm, $I_0 = 5 \times 10^{13}$ Wcm $^{-2}$, $\tau = 20$ fs and $w_0 = 49$ μ m.

Figure 6 (a) shows, in accordance with Fig. 4, a large increase in the ion yield with increasing polar angle for $\chi = 0^\circ$ as well as for the χ averaged result. For $\chi = 90^\circ$ the polarization vector is always directed in the molecular plane and by the argument given above the yield is generally much lower. In Fig. 6 (b) we see much the same trend for the MO-ADK model with the $\chi = 90^\circ$ geometries being suppressed compared with their $\chi = 0^\circ$ counterparts. Contrary to the results from the MO-SFA LG model, the yield is not maximized when polarization is perpendicular to the plane for $\chi = 0^\circ$ and χ averaged. The theories disagree because the tunneling rate is derived under the assumption that the electron emission only occurs close to the space-fixed Z axis determined by the linear polarization direction of the field. Hence, the MO-ADK rates reflect only the situation in this spatial region. For atoms, this is a reasonable assumption since the initial spherical symmetric potential will be affected most strongly in this direction and the potential barrier which arises from the combined field and atomic potential will then be minimized. For molecules, the initial potential is more complicated and the potential barrier can be minimized in other directions. Important contributions to the ion yield are thereby not taken into account and this is the reason why the results of the theories do not agree.

Since the tunneling ionization occurs close to the Z axis by assumption, the interpretation of the MO-ADK results can be made by analyzing the electron distribution in this direction. Previously, it was noted that the tunneling rate is largest when the initial electronic cloud is aligned with the field direction [23]. In Fig. 7 (a) we show a contour plot of the HOMO in the body fixed xz plane. When the field vector lies in this plane the geometry corresponds to $\chi = 0^\circ$ and with vertical and horizontal directions corresponding to $\theta = 0^\circ$ and $\theta = 90^\circ$,

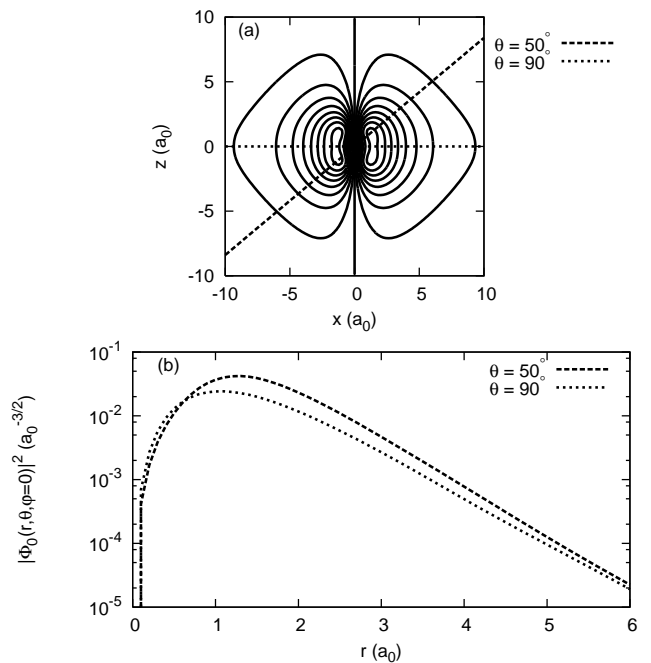


Figure 7: (a) Contour plot of the HOMO of ethylene in the xz plane. (b) The norm square of the HOMO along the directions $\theta = 50^\circ$ and $\theta = 90^\circ$. The unit of length is the Bohr radius $a_0 = 5.29177 \times 10^{-11}$ m.

respectively. To make it clear that $\theta = 90^\circ$ does not correspond to the largest electron density we have furthermore made a plot of $|\Phi_0(\mathbf{r})|^2$ along the directions $\theta = 50^\circ$ and $\theta = 90^\circ$ (Fig. 7 (b)). We clearly see that the electron density is largest for $\theta = 50^\circ$ at large distances. The minimum around $\theta = 90^\circ$ is also present in Fig. 6 (b) for the χ averaged yields.

B. Benzene

Benzene is a symmetric top molecule and hence it can only be aligned in the molecular plane [46] while it will be free to rotate around the body-fixed z axis (see Fig. 1 (b)). Thus only χ averaged signals as shown in Fig. 8 can be measured. We choose to present our calculated signals as a function of the angle, Θ , between the molecular plane and the polarization. Note that this angle is related to the usual Euler angle through the relation $\Theta = 90^\circ - \theta$ where θ is the polar angle between the Z -axis and the molecular plane in the frame defined in Fig. 1. This choice of data representation is convenient since a comparison with benzene derivatives like fluorobenzene and chlorofluorobenzene can be made more directly (Secs. VC and VD). In Fig. 8 we see that the MO-SFA LG model predicts the maximum yields at $\Theta = 42^\circ$ and $\Theta = 138^\circ$ while the MO-ADK model predicts maximum yields at $\Theta = 33^\circ$ and $\Theta = 147^\circ$. In both models the yield is minimized at $\Theta = 0^\circ$, 90° and 180° . These findings are in

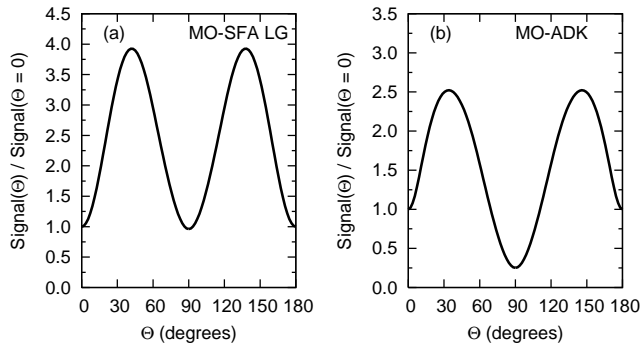


Figure 8: The orientational dependent ion signal for ionization of benzene as a function of $\Theta = 90^\circ - \theta$. The parameters of the laser are given in the caption of Fig. 6.

accordance with our expectations [2] since for $\Theta = 0^\circ$, 90° and 180° the polarization vector lies in a nodal plane and the asymptotic electron density is maximized in between. In a quantitative comparison between the models we find a somewhat larger modulation in the orientational dependent yield with the MO-ADK model than in the MO-SFA LG model.

C. Fluorobenzene

When one hydrogen atom in benzene is replaced by a fluorine atom, the six-fold rotational symmetry is broken and consequently the degeneracy of the HOMO is lifted. The doubly degenerate HOMO of benzene splits up in two components with the ionization potentials 9.35 eV and 9.75 eV. This energy difference is small compared with the energy separations to the other occupied orbitals and we will thus consider ionization from both orbitals.

Using the MO-SFA LG model, we present in Fig. 9 (a)–(c) the ion yields which originate from (a) the HOMO, (b) the second highest occupied orbital (HOMO–1) and (c) the integral yield from both channels. The figures 9 (d)–(f) contain equivalent results from the MO-ADK model. We find that the signals from both orbitals contribute significantly to the total signal and depending on the geometry, the contribution from either one will dominate. The relative importance between the ionization channels at a given geometry can be understood as a consequence of the symmetries of the orbitals.

Due to the C_{2v} symmetry of fluorobenzene the orbitals are eigenstates of the xz reflection operator with eigenvalues +1 (even) or –1 (odd). The reflection symmetry of an orbital is indicated by the subscript 1 for the even states and 2 for the odd states. The HOMO of fluorobenzene is a b_1 orbital, Fig. 1 (c), while the HOMO–1 is an a_2 orbital, Fig. 1 (d). Both orbitals are odd with respect to reflections in the molecular (yz) plane. Similar to ethylene, ionization of fluorobenzene is suppressed when $\chi = 90^\circ$ compared with the χ average since the

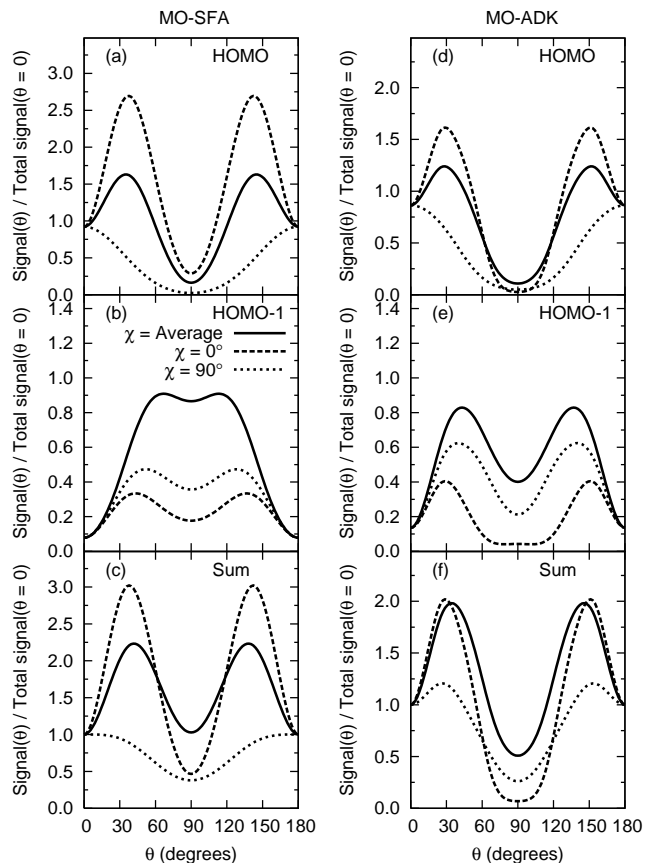


Figure 9: The orientational dependent ion signal for ionization from the highest occupied orbitals of fluorobenzene using MO-SFA LG (a)–(c) and MO-ADK (d)–(f). See Fig. 6 for details on the laser pulse and legends.

molecular plane is a nodal plane for both active orbitals. The b_1 orbital contains a non-planar nodal surface which is approximately parallel to the xy plane. When $\theta = 90^\circ$ the polarization is accordingly nearly parallel to this surface and we find the yield from the HOMO to be minimized around $\theta = 90^\circ$. The a_2 orbital is odd under the xz reflection and thus it contains a nodal plane in the xz plane. When the polarization is parallel to this plane ($\chi = 0^\circ$) we also find suppression of the ionization signal. In all cases we find qualitative agreement between the MO-SFA LG and MO-ADK results. In order to discuss the effect of the substitution of hydrogen with fluorine we note that the angles Θ for benzene and θ with $\chi = 0^\circ$ for fluorobenzene both describe the angle between the respective molecular planes and the polarization. It is thus relevant to compare the curve in Fig. 8 with the dashed curve in Fig. 9. In both theories we find that the total yield for fluorobenzene is slightly more suppressed around $\theta = 90^\circ$ than for benzene when it is compared with the maximum yields around 45 degrees (MO-SFA LG) and 30 degrees (MO-ADK).

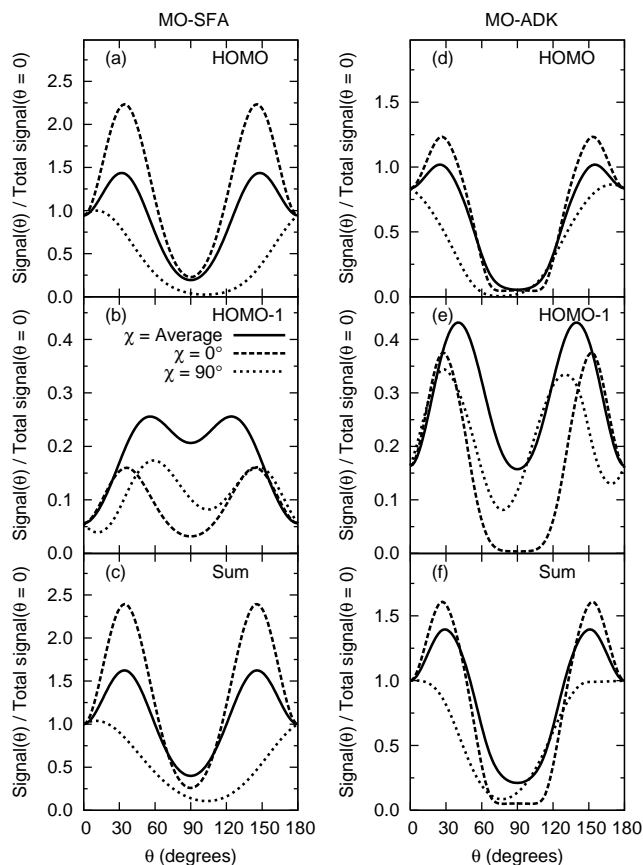


Figure 10: Similar to Fig. 9 but for chlorofluorobenzene.

D. Chlorofluorobenzene

In Fig. 10 we present the series of graphs for chlorofluorobenzene equivalent to the fluorobenzene results of Fig. 9. The ionization potentials that correspond to the two highest occupied orbitals are 9.37 eV and 9.80 eV, meaning that the energy difference between the HOMO and the HOMO-1 is 0.43 eV [47].

The molecular symmetry is reduced to contain only the reflection in the molecular plane as a symmetry operation (C_s point group) and, consequently, planar nodal surfaces can only lie in this plane. However, the two active orbitals of chlorofluorobenzene bear some similarities with their counterparts in fluorobenzene and thus our qualitative predictions will also be similar. The similar nodal surface structures can be seen by comparison of Figs. 1 (c)–(d) with Figs. 1 (e)–(f). The HOMO contains a nodal surface approximately parallel to the xy plane and the HOMO-1 contains a nodal surface approximately parallel to the xz plane. The similarities between the orbitals can be further exploited by comparing the asymptotic coefficients which are given in table I.

When we compare Figs. 9 and 10 we do indeed find alike behaviour. For the second highest orbital the suppression at $\chi = 0^\circ$ is now less pronounced. We can ex-

plain this phenomenon by the fact that the polarization is not parallel to a nodal plane but only approximately parallel to a nodal surface.

The most significant difference between the MO-SFA LG and the MO-ADK model is found at $\chi = 90^\circ$. Here the molecular plane lies parallel to the polarization and the angle θ determines how the molecule is rotated in this plane. In the MO-SFA LG model the total yield is minimized when $\theta > 90^\circ$ which corresponds to a geometry where the chlorine atom is directed along the polarization vector. In the MO-ADK model the minimum yield is found at $\theta < 90^\circ$ where the fluorine atom is directed along the polarization vector. We expect that this discrepancy arises from the fact that the tunneling theory only accounts for ionization in a narrow cylinder along the polarization direction of the field, as it is discussed in Sec. V A, and thus the MO-SFA LG model predicts the more accurate results.

VI. CONCLUSIONS AND OUTLOOK

In the present work, we have given a detailed account of the MO-SFA in the length gauge formulation, and we have presented the MO-ADK tunneling theory for non-linear polyatomic molecules. We have discussed the validity of the present effective single-electron models, and we have applied them to molecular systems where we expect the approach to be well justified. Indeed a comparison of our theoretical results with experimental ion-signal data for ethylene and benzene showed very good agreement, in particular in the length gauge formulation of the molecular strong-field approximation.

We have presented a detailed study of the characteristics of orientational-dependent ionization signals for ethylene, benzene, fluorobenzene, and chlorofluorobenzene, and thus covered systems with D_{2h} , D_{6h} , C_{2v} , and C_s point group symmetries. Our calculations of angular differential rates for ethylene showed that the distributions are largely determined by the nodal plane structure, and the comparison of predictions of the MO-ADK and the MO-SFA results for the orientational dependent ion signal for ethylene illustrated the shortcoming of the former model in accounting for situations where the ionization is peaked in other directions than along the polarization direction. The comparison of the orientational-dependent ion signals for the four different molecules showed that it is in general the nodal plane surfaces that determine the structure in the ionization yields. The point group of the molecules, although related, plays a less important role. An interesting feature, however, associated with the reduction in the point group symmetry is the lift of the degeneracy in the HOMO as we go from benzene to the substituted benzene molecules. In fluorobenzene and chlorofluorobenzene the energy difference between the HOMO and the HOMO-1 is comparably small, and one needs to consider ionization from both orbitals. The conclusions for the HOMO-1 with

respect to the importance of nodal surfaces remain unchanged. If one, on the other hand, speculates about possible experimental studies aiming at the separation and unique identification of HOMO and HOMO–1 dynamics, respectively, we propose to turn to a study of the photoelectron spectrum or above-threshold-ionization (ATI) spectrum. In the fixed–nuclei approximation applied throughout this work, we would see an ATI spectrum consisting of two series corresponding to electron energies which fulfil $q_n^2/2 = n\omega - E_b(j) - U_p$ with $E_b(j)$, ($j = \{\text{HOMO}, \text{HOMO}-1\}$) denoting the binding energies of the orbitals. Our present results show that depending on the molecular orientation, either one of the series will

lead to the stronger peaks. This effect is of course absent in benzene. Beyond the fixed–nuclei approximation, the ATI peaks will broaden due to coupling with the rovibrational degrees of freedom, and the different series may be impossible to distinguish. Whether this happens will be a study for the future.

Acknowledgments

LBM is supported by the Danish Natural Science Research Council (Grant No. 21-03-0163).

-
- [1] T. Brabec and F. Krausz, *Rev. Mod. Phys.* **72**, 545 (2000).
- [2] T. K. Kjeldsen, C. Z. Bisgaard, L. B. Madsen, and H. Stapelfeldt, *Phys. Rev. A* **68**, 063407 (2003).
- [3] V. R. Bhardwaj, D. M. Rayner, D. M. Villeneuve, and P. B. Corkum, *Phys. Rev. Lett.* **87**, 253003 (2001).
- [4] A. N. Markevitch, D. A. Romanov, S. M. Smith, H. B. Schlegel, M. Y. Ivanov, and R. J. Levis, *Phys. Rev. A* **69**, 013401 (2004).
- [5] M. J. DeWitt and R. J. Levis, *J. Chem. Phys.* **110**, 11368 (1999).
- [6] M. Lezius, V. Blanchet, D. M. Rayner, D. M. Villeneuve, A. Stolow, and M. Y. Ivanov, *Phys. Rev. Lett.* **86**, 51 (2001).
- [7] M. Lezius, V. Blanchet, M. Y. Ivanov, and A. Stolow, *J. Phys. Chem.* **117**, 1575 (2002).
- [8] G. G. Paulus, F. Grasbon, H. Walther, P. Villoresi, M. Nisoli, S. Stagira, E. Priori, and S. D. Silvestri, *Nature* **414**, 182 (2001).
- [9] M. V. Ammosov, N. B. Delone, and V. P. Krainov, *Sov. Phys. JETP* **64**, 1191 (1986).
- [10] L. V. Keldysh, *Sov. Phys. JETP* **20**, 1307 (1965).
- [11] F. H. M. Faisal, *J. Phys. B: At. Mol. Phys.* **6**, L89 (1973).
- [12] H. R. Reiss, *Phys. Rev. A* **22**, 1786 (1980).
- [13] S. F. J. Larochelle, A. Talebpoor, and S. L. Chin, *J. Phys. B: At. Mol. Opt. Phys.* **31**, 1215 (1998).
- [14] V. P. Krainov, *J. Opt. Soc. Am. B* **14**, 425 (1997).
- [15] L. B. Madsen, *Am. J. Phys.* (At print.).
- [16] I. V. Litvinyuk, K. F. Lee, P. W. Dooley, D. M. Rayner, D. M. Villeneuve, and P. B. Corkum, *Phys. Rev. Lett.* **90**, 233003 (2003).
- [17] J. Muth-Böhm, A. Becker, and F. H. M. Faisal, *Phys. Rev. Lett.* **85**, 2280 (2000).
- [18] J. Muth-Böhm, A. Becker, S. L. Chin, and F. H. M. Faisal, *Chem. Phys. Lett.* **337**, 313 (2001).
- [19] Z. X. Zhao, X. M. Tong, and C. D. Lin, *Phys. Rev. A* **67**, 043404 (2003).
- [20] T. K. Kjeldsen and L. B. Madsen, *J. Phys. B* **37**, 2033 (2004).
- [21] E. Eremina, X. Liu, H. Rottke, W. Sandner, M. G. Schatzel, A. Dreischuh, G. G. Paulus, H. Walther, R. Moshhammer, and J. Ullrich, *Phys. Rev. Lett.* **92**, 173001 (2004).
- [22] A. S. Alnaser, S. Voss, X. M. Tong, C. M. Maharjan, P. Ranitovic, B. Ulrich, T. Osipov, B. Shan, Z. Chang, and C. L. Cocke, *Phys. Rev. Lett.* **93**, 113003 (2004).
- [23] X. M. Tong, Z. X. Zhao, and C. D. Lin, *Phys. Rev. A* **66**, 033402 (2002).
- [24] H. D. Cohen and U. Fano, *Phys. Rev.* **150**, 30 (1966).
- [25] J. W. Robinson, ed., *Handbook of Spectroscopy* (CRC Press, Cleveland, Ohio, 1974).
- [26] M. Rittby and R. J. Bartlett, *J. Phys. Chem.* **92**, 3033 (1988).
- [27] E. P. Benis, J. F. Xia, X. M. Tong, M. Faheem, M. Zamkov, B. Shan, P. Richard, and Z. Chang, *Phys. Rev. A* **70**, 025401 (2004).
- [28] D. M. P. Holland, D. A. Shaw, M. A. Hayes, L. G. Shpinkova, E. E. Rennie, L. Karlsson, P. Baltzer, and B. Wannberg, *Chem. Phys.* **219**, 91 (1997).
- [29] P. Baltzer, L. Karlsson, B. Wannberg, G. Öhrwall, D. M. P. Holland, M. A. MacDonald, M. A. Hayes, and W. von Niessen, *Chem. Phys.* **224**, 95 (1997).
- [30] A. Jaroń-Becker, A. Becker, and F. H. M. Faisal, *Phys. Rev. A* **69**, 023410 (2004).
- [31] G. F. Gribakin and M. Y. Kuchiev, *Phys. Rev. A* **55**, 3760 (1997).
- [32] D. M. Brink and G. R. Satchler, *Angular Momentum* (Oxford University Press, London, 1968).
- [33] R. N. Zare, *Angular Momentum* (Wiley, New York, 1988).
- [34] B. M. Smirnov and M. I. Chibisov, *Sov. Phys. JETP* **22**, 585 (1966).
- [35] A. M. Perelomov, V. S. Popov, and M. V. Terent'ev, *Sov. Phys. JETP* **23**, 924 (1966).
- [36] C. Z. Bisgaard and L. B. Madsen, *Am. J. Phys.* **72**, 249 (2004).
- [37] M. W. Schmidt, K. K. Baldrige, J. A. Boatz, S. T. Elbert, M. S. Gordon, J. H. Jensen, S. Koseki, N. Matsunaga, K. A. Nguyen, S. J. Su, et al., *J. Comput. Chem.* **14**, 1347 (1993).
- [38] T. H. Dunning, *J. Chem. Phys.* **55**, 716 (1971).
- [39] T. Helgaker, P. Jørgensen, and J. Olsen, *Molecular Electronic-Structure Theory* (John Wiley & Sons Ltd, Baffins Lane, Chichester, 2000).
- [40] C. Eckart, *Phys. Rev.* **47**, 552 (1935).
- [41] M. Abramowitz and I. A. Stegun, eds., *Handbook of Mathematical Functions* (Dover Publications, Inc., New York, 1964).
- [42] B. Chang, P. R. Bolton, and D. N. Fittinghoff, *Phys. Rev. A* **47**, 4193 (1993).

- [43] A. Talebpour, A. D. Bandrauk, J. Yang, and S. L. Chin, *Chem. Phys. Lett* **313**, 789 (1999).
- [44] A. Talebpour, S. Laroche, and S. L. Chin, *J. Phys. B: At. Mol. Opt. Phys.* **31**, 2769 (1998).
- [45] S. Beiser, M. Klaiber, and I. Y. Kiyani, *Phys. Rev. A* **70**, 011402(R) (2004).
- [46] H. Stapelfeldt and T. Seideman, *Rev. Mod. Phys.* **75**, 543 (2003).
- [47] M. Mohraz, J. P. Maier, E. Heilbronner, G. Bieri, and R. H. Shiley, *J. Elec. Spec.* **19**, 429 (1980).